# Observation of Van Hove—type singularities in the local electron density of states by muon Knight-shift measurements in Cd and *Cd*Hg and *Cd*Mg alloys

W. Studer, F. N. Gygax, A. Hintermann, A. Schenck, and A. J. van der Wal
*Institute for Medium Energy Physics, Eidgenössische Technische Hochschule Zürich, c/o Schweizerisches Institut für Nuklearforschung, CH-5234 Villigen, Switzerland*
(Received 1 March 1984)

This paper contains a comprehensive account of positive-muon Knight-shift ($K_\mu$) measurements in the hcp metal Cd and the isostructural, isovalent alloys *Cd*Hg (1.23 at. % Hg) and *Cd*Mg (3.38 at. % Mg) which reveal a strong and peculiar temperature dependence never observed before by NMR Knight-shift studies. Most striking are anomalies in the temperature dependence which show up as a more or less resolved structure consisting of two "dips" and a "cusplike" (logarithmic) singularity in between. In pure monocrystalline Cd an axial Knight-shift contribution is observed which changes its sign precisely at the temperature at which the "cusplike" singularity is centered. The anomalies are shown to reflect Van Hove—type singularities in the local electron density of states. The number, sequence, and topological character of the singularities can be explained in terms of a three-band model, which is essentially a replica of the three-band model which describes the bulk band structure of Cd and its Hg and Mg alloys close to the Fermi energy in the vicinity of the $K$-symmetry point in the hcp Brillouin zone. Quite unexpected and unexplained so far is the observation that, compared to the bulk band structure, the present "band states" display a reduced splitting and are considerably down-shifted relative to the Fermi energy, both effects being dependent on the alloy composition. This seems to be a new phenomenon induced locally by the presence of an interstitial and single hydrogenlike impurity.

## I. INTRODUCTION

The use of the positive muon ($\mu^+$) as a local probe of electronic properties of metallic systems is interesting from mainly two points of view. First, the electrostatic interaction of the $\mu^+$ with the environment is much like that of a proton. If one neglects isotope effects, the induced electronic structure around either particle is expected to be identical. This fact is exploited when muon-spin-rotation ($\mu$SR) observations are used to better comprehend the local electronic structure of hydrogen in metals.[1]

Second, the $\mu^+$ prefers a position in the lattice far from the positively charged host ions, viz., an interstitial site. It therefore samples a spatial region largely inaccessible to techniques such as NMR, neutron scattering, or Mössbauer spectroscopy. This opens the possibility of studying the host material from a new and complementary point of view.

In this paper we report on a detailed investigation of the temperature and orientation dependence of the muon Knight shift $K_\mu$ or the induced hyperfine field at the $\mu^+$ in the hcp metal Cd and the isostructural, isovalent *Cd*Hg (1.23 at. % Hg) and *Cd*Mg (3.38 at. % Mg) alloys. Anticipating the results, it is found that both aspects mentioned are involved in an unexpected, interrelated manner, constituting a new effect.

A review of previous $K_\mu$ measurements in nonmagnetic metals and transition metals can be found in Ref. 1. Several mechanisms contribute to the Knight shift: (i) the direct or Fermi-contact contribution $K_s$ from spin-polarized conduction electrons, (ii) the so-called "core-polarization" contribution $K_{CP}$ from electronic states below the Fermi level which are spin-polarized by exchange and correlation with the Fermi-surface conduction electrons, and (iii) the diamagnetic screening contribution $K_{dia}$. Theoretical model calculations are necessary to split $K_\mu$ into the various contributions and to discuss it in terms of the local electronic structure. The most successful model calculations on the systematics of $K_\mu$ in simple monovalent and divalent metals were made by Manninen[2] within the framework of the spherical solid model (SSM), which is a refined jellium model. The success of the SSM originates from the proper inclusion of the host-ion potentials spherically averaged in the lattice geometry around the site of residence of the muon.

In nontransition metals the contact contributions $K_s$ and $K_{CP}$ are commonly combined in the expression $K_s+K_{CP}=\frac{8}{3}\pi\rho\langle\chi_s\rangle$. $\rho$ is the spin-density enhancement factor at the muon site and reflects the local aspect of the induced electron structure, whereas $\langle\chi_s\rangle$ is the bulk spin susceptibility properly averaged over the Fermi surface. In nontransition metals, $K_\mu$ is expected to be essentially independent of temperature. This has been confirmed by measurements of $K_\mu$ in Cu (Ref. 1) and Al (unpublished).

The strong Coulomb potential of a proton is screened in a metal by conduction electrons which are assumed to possess mainly $s$-electron character with respect to the impurity. In PdH the partial densities of states within the hydrogen cell show that the $s$ part dominates by far over $p$ or $d$ parts.[3] Measurements of the Dingle temperature in the de Haas—van Alphen effect on dilute $Cu\mathrm{H}_x$ (Ref. 4) show that the screened proton constitutes a short-range, essentially structureless isotropic scattering center for the

 

conduction electrons. Non-$s$ parts in the local-electron distribution can give rise to anisotropic hyperfine-field contributions via the dipolar coupling between the proton and electron spins, provided that the relevant symmetry is noncubic.

The isotropic Fermi-contact interaction may also display anisotropy if the relevant spin susceptibility is anisotropic. The latter originates from an anisotropic $g$ factor which, in turn, is the result of spin-orbit coupling. The observation of an anisotropic Knight shift may therefore provide the possibility of studying such effects.

The divalent, weakly diamagnetic metal Cd with its hcp lattice structure is an interesting system by itself. Its large $c/a$ ratio of 1.88 deviates far from the ideal value of 1.63 and accounts for strong anisotropies in many properties and also, in part, for the complicated band structure. Theoretically, the band structure of Cd has been studied in detail.[5] Spin-orbit coupling is responsible for the energy splitting of otherwise degenerate states along certain symmetry lines, in particular at the symmetry point $K$ (the center of the vertical edges of the hexagonal Brillouin zone of the hcp lattice). The electron states near symmetry point $K$ strongly influence the susceptibility component parallel to the $c$ axis both in Cd (Refs. 6 and 7) and in the isostructural, isovalent *Cd*Hg and *Cd*Mg alloys (Refs. 7–9). This can be theoretically understood on the basis of a three-band model which describes the band structure near symmetry point $K$.[7] This three-band model involves three closely spaced bands with critical points close to the Fermi energy. The position of the Fermi level in Cd relative to these critical-energy points depends sensitively on the $c/a$ ratio. The interest in the isostructural, isovalent Cd alloys is motivated by the possibility of controlling the position of the Fermi level relative to the critical points by varying the alloy composition which, in turn, determines the $c/a$ ratio.

The unusual hyperfine properties of Cd and its alloys have been extensively studied by means of nuclear magnetic resonance.[10] The Cd nuclear Knight shift, sampling electronic properties at the regular lattice site, shows a strong temperature dependence of the isotropic and axial parts not observed in other nontransition metals. Kasowski[11] proposed an explanation for this behavior on the basis of the electron-phonon interaction which changes the Cd pseudopotentials. For a more recent theoretical calculation of the Cd nuclear Knight shift, see Ref. 12. In contrast to the total susceptibility, the Cd nuclear Knight shift is not affected by the electron states near symmetry point $K$.[11] Attempts to calculate the Pauli spin susceptibility for Cd, essential in the analysis of hyperfine properties, can be found in Refs. 11 and 13. In addition, one observes a discontinuous increase of 33% upon melting in the nuclear Knight shift of Cd. This is ascribed to a jump in the density of states or in the spin susceptibility, respectively.[11,14] The present $\mu^+$ Knight-shift results follow distinctively different patterns and seem, in contrast to the Cd nuclear Knight shift, to be strongly correlated with features of the Cd band structure near symmetry point $K$. The present study is the first on a hydrogenlike interstitial impurity in Cd. In this respect it should be noted that the hydrogen solubility of Cd is quoted to be zero up to 670 K.[15]

The paper is organized as follows. In Sec. II we deal with the experimental details. A brief account of the band structure around symmetry point $K$ is given in Sec. III, where we also discuss Van Hove singularities, which are important for the explanation of anomalies observed in $K_\mu$. In Sec. IV A we present the measurements of the isotropic and axial part of $K_\mu$ in pure Cd, both of which are strongly temperature dependent. Around 110 K, anomalous contributions to $K_\mu$ are observed in Cd. More insight into this phenomenon is obtained from measurements in a polycrystalline *Cd*Hg (1.23 at. % Hg) sample (Sec. IV B) and in a polycrystalline *Cd*Mg (3.38 at. % Mg) sample (Sec. IV C). In Sec. V the experimental results are discussed. A summary, Sec. VI, concludes the paper.

## II. EXPERIMENTAL DETAILS

### A. Samples

Table I describes the samples and their origin. The single crystals were oriented with the aid of x-ray Laue patterns. Atomic absorption spectral analysis yielded a Mg concentration of 3.38 at. % in the *Cd*Mg specimen and a Hg concentration of 1.23 at. % in the *Cd*Hg specimen.

### B. Measurements

The measurements were performed at the superconducting muon channel of the Swiss Institute for Nuclear Research (SIN). Positive muons were stopped in the samples listed in Table I inside a cryostat or an oven in a highly homogeneous magnetic field of 0.747 T, stable to

TABLE I. Sample description. (SC denotes single crystal.)

| Sample | Form | Diameter(×length) mm(×mm) | Purity (%) | source |
|---|---|---|---|---|
| Cd | polycrystalline sphere | 25 | 99.9999 | a |
| Cd(SC) | monocrystalline sphere | 24 | 99.999 | b |
| Cd(cyl) | monocrystalline cylinder | 28×40 | 99.999 | b |
| *Cd*Hg (1.23 at. % Hg) | polycrystalline cylinder | 25×50 | 99.999 | a |
| *Cd*Mg (3.38 at. % Mg) | polycrystalline cylinder | 25×50 | 99.999 | a |

[a]Metals Research.
[b]Atomergic Chemetals.

better than 1 ppm. The stroboscopic technique[16] was used to observe the muon-precession frequency $\omega_\mu$. The applied field was measured by proton ($H_2O$) NMR in terms of $\omega_p$, the proton-resonance frequency. The Knight-shift value $K_\mu$ is then calculated from the ratio $\omega_\mu/\omega_p$ with help of the following expression:[1]

$$K_\mu=\left[\frac{\omega_\mu}{\omega_p}\right]\left[\frac{\mu_\mu}{\mu_p}\right]^{-1}(1-\sigma_{H_2O})+\left[N-\frac{4\pi}{3}\right]\chi_b-1\ . \tag{1}$$

$\mu_\mu/\mu_p=3.183\,344$ is the ratio of the muon and proton magnetic moments and is known to $\pm 0.5$ ppm.[16] $\sigma_{H_2O}=25.6$ ppm denotes the diamagnetic shielding constant for protons in water. $\chi_b$ is the bulk magnetic susceptibility and $N$ is the demagnetization factor of the sample. Using a spherical sample with $N=4\pi/3$, the term containing $\chi_b$ vanishes. The stroboscopic resonance curves were scanned back and forth over a field ranging from $\omega_p=31.71$ to 31.91 MHz, or about 3 times the linewidth $1/(\pi\tau_\mu)=1500$ ppm, in 25 steps. Typically, $6\times10^6$ muon-decay counts per field point were accumulated, which resulted in a statistical error of 3–4 ppm. The statistical error dominates, by far, the uncertainties due to field regulation, field measurements, and field homogeneity over the target volume which, together, total from 0.8 to 1.2 ppm. Inside the cryostat a diamagnetic shielding of $-5$ ppm was measured and subtracted as a correction in the $K_\mu$ value. A He-flow cryostat, stabilized to better than 0.25–1 K, depending on the temperature range, was used to vary the temperature from 4.2 to 350 K. Above room temperature an oven operating with a heated $N_2$-gas flow was used; its temperature stability was typically between 1 and 3 K.

The stroboscopic technique essentially consists of counting the positron rate as a function of the applied field in a certain time window, which is phase-locked to the beam-burst repetition frequency $\Omega/2\pi=50.63$ MHz. For muons whose polarization decays with an exponential function $\exp(-t\lambda)$, these so-called stroboscopic signals are given by Lorentzian line-shape functions,

$$N_{e+}=N_0\left[1+A_{\rm eff}\left[\cos\varphi\frac{1}{1+(\omega_\mu-2\Omega)^2\tau_{\rm eff}^2}+\sin\varphi\frac{(\omega_\mu-2\Omega)\tau_{\rm eff}}{1+(\omega_\mu-2\Omega)^2\tau_{\rm eff}^2}\right]\right],$$
$$1/\tau_{\rm eff}=\lambda+1/\tau_\mu\ . \tag{2}$$

Here, $N_0$ is a normalization constant, $A_{\rm eff}$ is the effective muon-decay asymmetry, $\varphi$ is the mixing angle, $\tau_{\rm eff}$ is the effective lifetime, $\tau_\mu$ is the muon lifetime, $\omega_\mu$ is the muon-precession frequency and $2\Omega/2\pi=101.3$ MHz is the reference frequency with which $\omega_\mu$ is compared. To take into account the dipolar broadening of the signals due to the nuclear magnetic moments of Cd, the stroboscopic signals below 80 K were also analyzed with the expression

$$N_{e+}=N_0\left[1+A_{\rm eff}\left[\cos\varphi\int_{-\infty}^{+\infty}P(\omega')\frac{d\omega'}{1+(\omega_\mu+\omega'-2\Omega)^2\tau_\mu^2}+\sin\varphi\int_{-\infty}^{+\infty}P(\omega')\frac{(\omega_\mu+\omega'-2\Omega)\tau_\mu d\omega'}{1+(\omega_\mu+\omega'-2\Omega)^2\tau_\mu^2}\right]\right]. \tag{3}$$

Here,

$$P(\omega')=(4\pi\sigma^2)^{-1/2}\exp(-\omega'^2/4\sigma^2)$$

is the Gaussian frequency distribution which corresponds to a Gaussian relaxation function in time space, or $R(t)=\exp(-\sigma^2t^2)$. The damping constant $\sigma$ is related to the second moment $M_2$ of the nuclear-dipolar-field spread, $\sigma=(M_2/2)^{1/2}$. $\sigma$ amounts to $\sim0.02$ $\mu$sec$^{-1}$ and contributes little to the linewidth of the signals.

## III. ELECTRONIC PROPERTIES OF Cd

### A. Band structure at symmetry point $K$

In metal Cd, anomalies in electronic properties are most likely expected to originate from electron states near the symmetry point $K$, where three closely spaced bands exist with critical points close to the Fermi surface. In the free-electron approximation the electron state at $K$ is threefold degenerate. The electrostatic energy $E_c$ of the crystal field partially lifts this degeneracy and splits the state into a lower band and two upper bands which are still degenerate at $K$. Spin-orbit coupling removes this degeneracy further and splits the upper bands at $K$ symmetrically by $\pm\Delta/3$ where $\Delta$ is the spin-orbit energy. The band structure around $K$ can be described by a Bennet-Falicov model which is a $\vec{k}\cdot\vec{p}$ or Taylor expansion around $K$.[7,17] This three-band model involves velocity matrix elements $A,B$, an electrostatic splitting energy $E_c$, and a spin-orbit energy $\Delta$ as phenomenological parameters. For pure Cd, the following values are quoted:[7] $A=(0.94$ Ry$)a_B$, $B=(0.97$ Ry$)a_B^2$, $E_c=0.0192$ Ry, and $\Delta=0.012\,12$ Ry; $a_B$ is the Bohr radius. McClure *et al.*[7] obtained, from their analysis of the concentration dependence of the low-temperature susceptibility data in *Cd*Hg and *Cd*Mg,[8] with a simplified Bennet-Falicov model, the parameters $E_c=0.009$ Ry and $\Delta=0.018$ Ry (Ref. 18) [$A=(1.00$ Ry$)a_B$ and $B=(1.00$ Ry$)a_B^2$], in good agreement with Ref. 5.

In general, one has four critical points, i.e., where $\mathrm{grad}_{\vec{k}}E(\vec{k})=0$, in this three-band model. Three of these are found at $K$ (labeled $E_1,E_2,E_3$), whereas the remaining critical point ($E_L$) of the intermediate band may be found either along symmetry line $\Gamma M$ or $\Gamma K$. In Table II the critical points expressed in terms of $E_c$ and $\Delta$ are summarized as given by McClure,[7] together with their three-dimensional (3D) and two-dimensional (2D) ($k_x$-$k_y$ plane) topology.

For $\Delta/E_c=1$, the critical points $E_2$ and $E_L$ of the in-

TABLE II. Critical points of the three-band model with $E_1$ as the origin of the energy scale and their topological 3D character and topological 2D character in the $k_x$-$k_y$ plane.

| Band | Critical point | 3D | 2D |
|---|---|---|---|
| lower band | $E_1=0$ | $M_2$ saddle point | maximum |
| intermediate band | $E_2=E_c-\Delta/3$ | $M_0$ minimum | minimum |
| | $E_L=8E_c\Big/\left\{9\left[1+\left[\frac{\Delta}{E_c}\right]^2\frac{1}{3}\right]\right\}$ | $M_1$ saddle point | saddle point |
| upper band | $E_3=E_c+\Delta/3$ | $M_0$ minimum | minimum |

termediate band degenerate to a single saddle point. For $\Delta/E_c<1$, $E_L$ is smaller than $E_2$, and for $\Delta/E_c>1$, $E_L$ is larger than $E_2$, but in both cases, very close to $E_2$.

### B. Critical points and Van Hove singularities

As is well known, critical points give rise to Van Hove singularities[19] in the electron density of states. A thorough discussion of the occurrence of critical points by topological and symmetry arguments is given in Refs. 19 and 20. Analytical critical points have a Taylor expansion around $E_{cr}$, which is quadratic in $\vec{k}$ to lowest order. A complete classification of analytical critical points in two and three dimensions and the types of singularities they produce in the density of states for energies $E$ close to the critical energy $E_{cr}$ can be found in Ref. 19. Nonanalytical critical points, where some of the components of $\text{grad}_{\vec{k}}E(\vec{k})$ are zero and others are discontinuous, are extensively discussed in Ref. 20. The characteristic contribution of analytical critical points in two dimensions to the density of states, $\Delta g(E)$, are (i) finite discontinuities for minima and maxima where the discontinuous step depends on the curvature of $E(\vec{k})$ at $E_{cr}$, and (ii) logarithmic singularities for saddle points, i.e., $\Delta g(E)\propto\ln|E/E_{cr}-1|$. In three dimensions the density of states $\Delta g(E)$ near analytical critical points typically shows a square-root behavior, e.g., $\Delta g(E)\propto\pm|E-E_{cr}|^{1/2}$, for either $E>E_{cr}$ or $E<E_{cr}$. This is illustrated in the inset of Fig. 10 where the density-of-states curve is represented in its 3D (dotted line) and its 2D $k_x$-$k_y$—plane (solid line) form as calculated from the three-band model for the electrons near symmetry point $K$, according to Ref. 7. A 2D density of states is expected whenever the energy dispersion does not or only weakly depends on one of the components of $\vec{k}$.

A change in the lattice parameters of the crystal by thermal expansion, stress, or alloying may change the position of the Fermi level $E_F$ relative to the critical points and thus lead to electronic anomalies as a function of temperature, stress, or the alloy composition. The change in the topology of the Fermi surface when passing a critical point is called "electron phase transition" or "Lifshitz phase transition."[21]

### C. Experimental evidence for a Lifshitz phase transition in Cd and Cd alloys involving symmetry point $K$

Experimental evidence for a Lifshitz phase transition in Cd and Cd alloys involving symmetry point $K$ follows exclusively from measurements of the total susceptibility $\chi_{tot}$.[7–9] Svechkarev and co-workers[8] have discovered interesting structures in the susceptibility component $\chi_{\|}$ parallel to the $c$ axis of Cd alloys (see Fig. 1). These structures are traced back by McClure *et al.*[7] to the orbital contribution to $\chi_{tot}$ from electron states near symmetry point $K$ and to the effect of the passage of the Fermi level $E_F$ through the critical-energy points associated with symmetry point $K$. In this analysis the band structure at symmetry point $K$ was assumed to be rigid and represent-

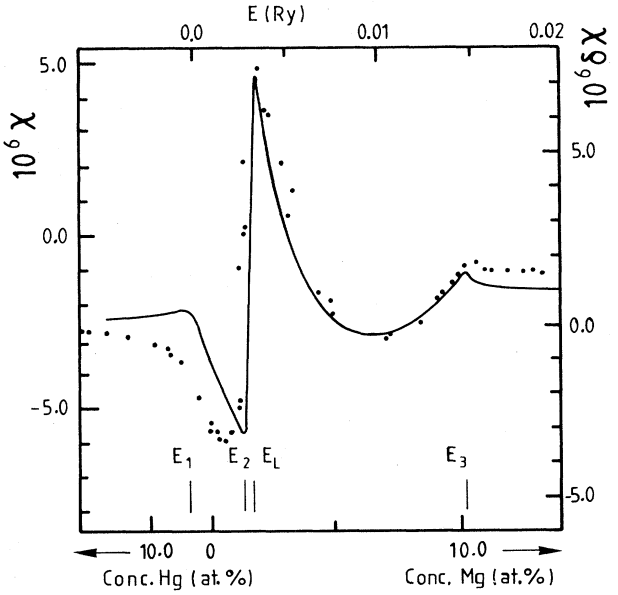


FIG. 1. Magnetic susceptibility of Cd alloys at 4.2 K for the magnetic field parallel to the $c$ axis. The points are the data of Svechkarev and Kuzmicheva (Ref. 8) plotted vs a scale which is roughly proportional to the $c/a$ ratio. The lower and left scales refer to the experimental data. The solid curve is from the theory of Ref. 7. The upper and right scales refer to the theory. The susceptibility is in units of emu/cm$^3$. Both susceptibility plots have the same scaling factor, but are offset by $2.56\times10^{-6}$ emu/cm$^3$.

ed by the three-band model discussed above. The orbital contributions to $\chi_{\parallel}$ depend strongly on the position of the Fermi level relative to the critical points. In pure Cd, $E_F$ falls between the energy points $E_1$ and $E_2$. When the $c/a$ ratio is increased by either raising the temperature or alloying the isoelectronic Hg to Cd, the Fermi level is shifted to lower energies. On the other hand, a decreasing $c/a$ ratio obtained by alloying the isoelectronic Mg to Cd shifts $E_F$ toward higher energies and leads to the structures on the right-hand side of Fig. 1, which reflect the passage of $E_F$ through $E_2$, $E_L$, and $E_3$.

Electrons at symmetry point $K$ do not contribute to the de Haas–van Alphen signal in pure Cd, a consequence of the position of $E_F$ between the $E_1$ and $E_2$ critical points at $T=0$ K. This is in contrast to the situation in hcp Zn ($c/a=1.86$) where, at $T=0$ K, $E_F$ is known to fall in the upper band with the $E_3$ minimum. In Zn, these tiny electron pockets of the upper band, the so-called "needles," have a very small effective mass and a small extremal area perpendicular to the $c$ axis, and manifest themselves in pronounced de Haas–van Alphen oscillations.[22]

The absence of anomalies originating from electrons near symmetry point $K$ in the Cd nuclear Knight shift in Cd and Cd alloys is discussed in Sec. V.

## IV. EXPERIMENTAL RESULTS

### A. Cadmium

#### *1. Temperature dependence*

Figure 2 shows the temperature dependence of $K_\mu$ in the polycrystalline Cd sample between 20 K and the melting temperature ($T_m=593$ K) as well as a few data points in the liquid state. The overall behavior is indicated by the dotted line below 150 K and the solid line above 150 K. The very large increase of $K_\mu$ with temperature is extraordinary for a weakly diamagnetic metal and unique compared with $K_\mu$ in other nontransition metals.[1] Assuming a temperature-independent diamagnetic contribution[23] $K_{\rm dia}\cong -20$ ppm, the spin part of $K_\mu$ increases by more than 100% between $T=0$ K and $T_m$. A temperature dependence in $K_\mu$ of this extent is commonly found only in $3d$ (Ref. 24), $4d$ (Ref. 25), or $5d$ (Ref. 26) transition metals, or in intermetallic compounds of rare-earth metals[27] where $K_\mu$ scales with the susceptibility of the $3d$, $4d$, $5d$, or $4f$ electrons. In Cd, $K_\mu$ definitely does not scale with the total bulk susceptibility which also increases with $T$, but is known to be dominated by orbital contributions.[7] The temperature dependence shows that $K_\mu$ in Cd obviously cannot be accounted for by a theory based on the jellium or free-electron approach since no temperature dependence exists in such theories. The pro-

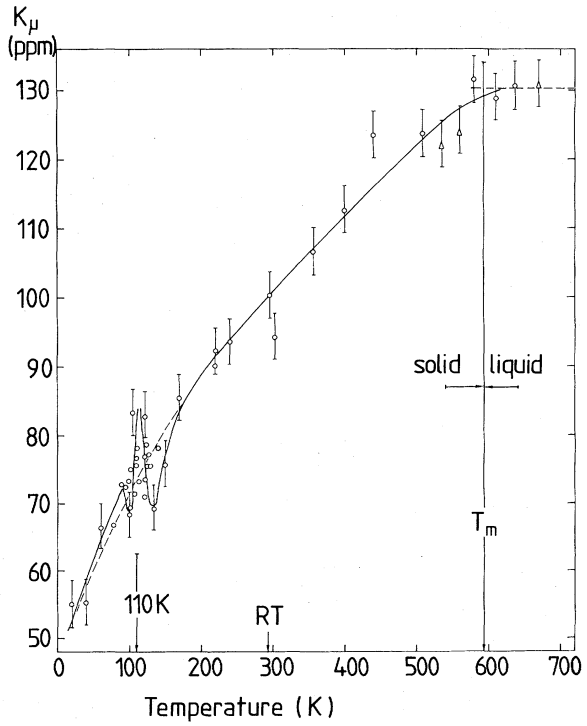


FIG. 2. Isotropic muon Knight shift $K_\mu$ in the solid and liquid phases of a polycrystalline Cd sample between 20 and 660 K (melting temperature $T_m=593$ K; RT denotes room temperature).

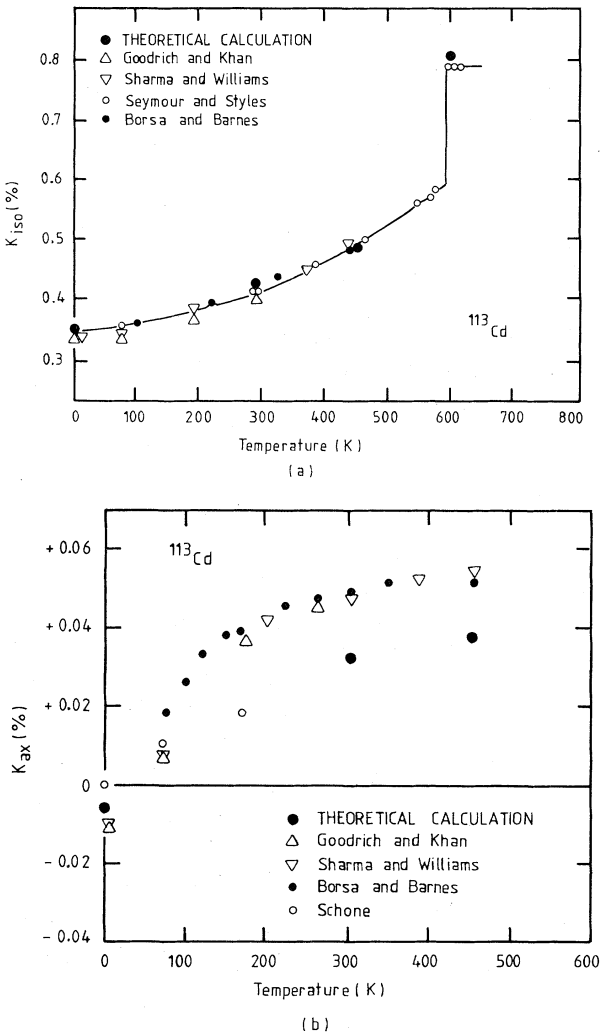


FIG. 3. (a) Experimental and theoretical isotropic nuclear Knight shift in Cd as a function of temperature (from Ref. 11). (b) Experimental and theoretical axial nuclear Knight shift in Cd as a function of temperature (from Ref. 11).

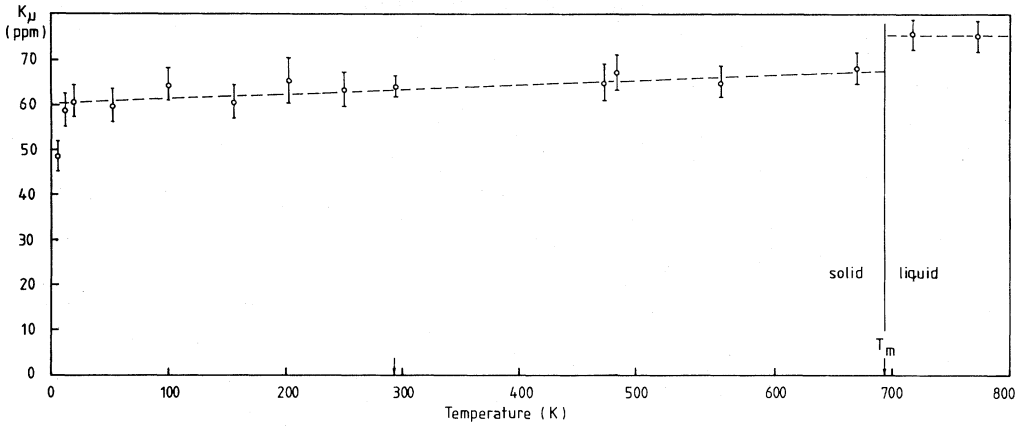


FIG. 4. Isotropic muon Knight shift in the solid and liquid phases of Zn (melting temperature $T_m = 692$ K).

nounced increase of $K_\mu$ with $T$ also exceeds, by far, the similarly unusual temperature behavior of the isotropic part of the Cd nuclear Knight shift shown in Fig. 3(a). The explanation proposed in Ref. 11 for the nuclear Knight shift in Cd is primarily based upon the influence of the electron-phonon coupling on the Cd pseudopotentials. $K_\mu$ in Cd should also be compared with the isotropic muon Knight shift in hcp Zn, which possesses a nearly identical $c/a$ ratio and electronic properties very similar to Cd. $K_\mu$ in Zn rises only slightly and linearly with $T$ (see Fig. 4) according to

$$K_\mu(T) = K_0 + \frac{\partial K}{\partial T} T \,,$$
$$K_0 = (60.3 \pm 1.7) \text{ ppm} \,, \tag{4}$$
$$\frac{\partial K}{\partial T} = [(1.1 \pm 0.45) \text{ ppm}]/100 \text{ K} \,.$$

### 2. *Anomalous Knight-shift contributions*

The second and, as will be shown, most interesting aspect of $K_\mu$ in Cd, concerns the anomalous structures observed around 110 K (see Fig. 2). The cusplike singularity accompanied by minima to the left and right is more clearly resolved in measurements with a single-crystal sample (Fig. 5). The solid circles in Fig. 5 represent $K_\mu$ with the external field parallel to the $c$ axis ($K_{||}$) and the open circles correspond to the orientation perpendicular to the $c$ axis ($K_\perp$) for temperatures from 20 to 550 K. The sharp singularity at 110 K and the fine structure of this anomalous $K_\mu$ contribution are confined to a narrow temperature interval and are present in both orientations. The anomaly is distinctively different from broader structures which can be related to diffusion and trapping at crystalline defects.[28] This unique feature of $K_\mu$ in Cd must clearly originate from an electronic peculiarity of the host metal Cd, since the Knight shift samples electronic properties such as the electron density, the electronic spin density, or the density of states (via the spin susceptibility). The fact that the singularity occurs both in the single-crystal sample independently of orientation as well as in the polycrystalline sample indicates that a scalar property is involved.

In addition, the particular temperature of 110 K, as can be seen from Figs. 2 and 5, also marks a pronounced change in the slope $\partial K_\mu/\partial T$ from a steep behavior below 110 K to a less steep behavior above 110 K. In Cd the most likely candidates for anomalies in electronic properties are electron states near the symmetry point $K$ of the hexagonal Brillouin zone of the hcp lattice, as was discussed in the preceding section. Their strong influence on the diamagnetic susceptibility was mentioned there. In Sec. V we will show that the anomalous muon Knight shift in Cd seems to map Van Hove singularities in the local-electron density of states associated with the band structure near symmetry point $K$.

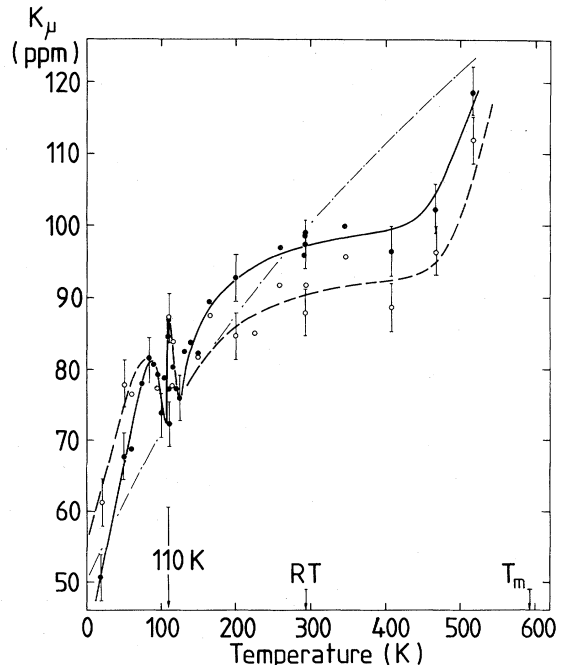


FIG. 5. $K_\mu$ in a Cd single crystal [Cd(SC) sample] between 20 and 520 K for the applied field parallel ($K_{||}$, solid circles) and perpendicular ($K_\perp$, open circles) to the $c$ axis. The dashed-dotted line indicates the overall temperature dependence of $K_\mu$ in the polycrystalline sample of Fig. 2. The solid and the dashed lines are guides to the eye.

### 3. *Anisotropic contributions to* $K_\mu$

As shown in Fig. 5 the muon Knight shift depends on the orientation of the $c$ axis with respect to the applied field; hence, the local field at the muon site does not follow the external field. The observed angular dependence of $K_\mu$ in Fig. 6 at $T=60$ and 30 K fits the expression

$$K_\mu(T,\vartheta)=K_{\rm iso}(T)+K_{\rm ax}(T)(3\cos^2\vartheta-1)\ , \qquad (5)$$

where $\vartheta$ is the angle between the applied field and the sixfold $c$ axis.[29] This is the most general, lowest-order angular contribution allowed by symmetry for a muon ensemble residing at regular interstitial octahedral or tetrahedral sites in the hcp lattice. The interesting temperature dependence of the axial part, $3K_{\rm ax}=K_{||}-K_\perp$, which results from a point-by-point subtraction of the data in Fig. 5, is presented in Fig. 7. At roughly 110 K, $K_{\rm ax}$ vanishes. Below 110 K, $K_{\rm ax}$ is negative and amounts to $-3$ to $-4$ ppm at $T=0$ K; above 110 K, $K_{\rm ax}$ is positive and temperature independent with $+2$ ppm over a wide temperature interval between 250 and 510 K. It should be mentioned that the single-crystal sample investigated originally[30] showed a much larger reproducible $K_{\rm ax}$ at room temperature, amounting to $\sim+7$ ppm (also see Ref. 29). The origin of this inconsistency is not known. The change in sign at about 110 K correlates with the anomalous cusp singularity and appears, therefore, to be intimately related to the same origin as the singularity. For comparison, the axial nuclear Cd Knight shift is shown in Fig. 3(b).

### 4. $K_\mu$ *in the melt*

In the preceding section on the $K_\mu$ results in the solid state of Cd, it was suggested that $K_\mu$ is strongly influenced by the properties of the ordered crystalline state of the host. Subsequently, we have also measured $K_\mu$ in the liquid state of Cd, which is believed to display free-electron characteristics.[11] The three data points taken in the melt between $T_m=593$ and 660 K are shown in Fig. 2. In the liquid state, $K_\mu$ is (131±2) ppm. This value is approached smoothly in the solid state upon approaching the melting point. This behavior is in clear contrast with the Cd nuclear Knight-shift results, where a sharp and

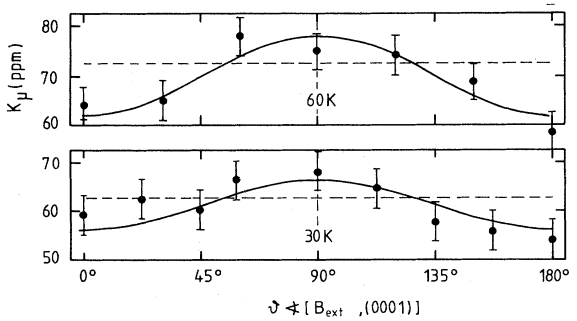


FIG. 6. Explicit angular dependence of $K_\mu$ at 30 and 60 K. $\vartheta$ refers to the angle between the applied field and the $c$ axis of the Cd(SC) sample. Solid lines are fits to $K_\mu(T,\vartheta)=K_{\rm iso}(T)+K_{\rm ax}(T)(3\cos^2\vartheta-1)$. The isotropic part $K_{\rm iso}=(K_{||}+2K_\perp)/3$ is given by the dashed horizontal lines.

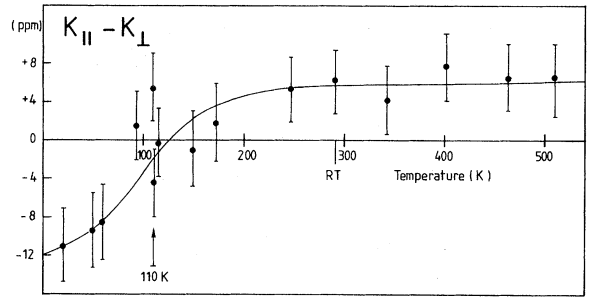


FIG. 7. Temperature dependence of the axial part $3K_{\rm ax}=K_{||}-K_\perp$ between 20 and 520 K in the Cd(SC) sample obtained by a point-by-point subtraction of the data in Fig. 5.

finite rise of 33% for the isotropic part in the melt is reported.[10] Ziman[14] and Kasowski[11] ascribe this large increase upon melting to a change in the spin susceptibility or the density of states at the Fermi level, respectively. In the analysis of muon Knight-shift data it was so far always assumed, after a proper correction for the diamagnetic screening constant $K_{\rm dia}$, that $K_\mu$ scales with the bulk spin susceptibility of the host metal.

In Zn, in contrast, $K_\mu$ is found to increase slightly by about (12±7)% in the melt (Fig. 4). In Zn no NMR data above liquid-He temperature are reported owing to the low natural abundance of the only Zn isotope with a nonzero nuclear magnetic moment (spin $\frac{3}{2}$) and to strong quadrupolar coupling in the hexagonal lattice.

The missing discontinuity in $K_\mu$ upon melting in Cd can therefore be taken as the first experimental indication that the interstitial $\mu^+$ Knight shift does not necessarily scale with the bulk spin susceptibility.

## B. *Cd*Hg

Additional information about the nature of the anomalous muon Knight shift in pure Cd is expected to be obtained from measurements in isostructural, isovalent dilute *Cd*Hg alloys. In particular, it may tell if the anomaly of $K_\mu$ in Cd originates from features of the Cd band structure associated with the electron states near symmetry point $K$. In Fig. 8 we have plotted the four critical energy points $E_1$, $E_2$, $E_L$, and $E_3$ near $K$ and the approximate position of the Fermi level $E_F$ at $T=0$ K following Ref. 7 for pure Cd and *Cd*Hg (2 at. % Hg). Alloying the isoelectronic Hg, with its slightly larger ionic radius, to the Cd matrix, increases the $c/a$ ratio of the hexagonal lattice and, consequently, shifts the Fermi level toward lower energies, or closer to $E_1$. Similarly, raising the temperature increases the $c/a$ ratio and shifts the Fermi level to lower energies. Since at 0 K in *Cd*Hg the Fermi level is somewhat lower than in pure Cd, we naively expect, for the *Cd*Hg sample, a shift of the anomalous cusp towards lower temperature as compared to the Cd sample.

We now estimate the expected temperature shift with use of the susceptibility data of pure Cd (Ref. 6) and the concentration dependence of the susceptibility in *Cd*Hg ($x$ at. % Hg) (Ref. 8). The change in slope of the Cd susceptibility occurs at about 110 K and corresponds, in the

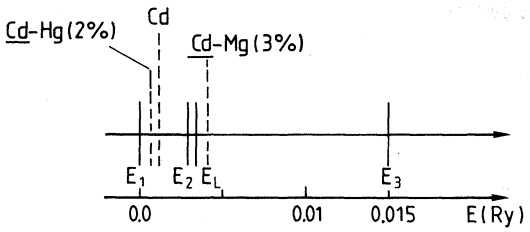


FIG. 8. Critical energies $E_1$, $E_2$, $E_L$, and $E_3$ in Ry according to Ref. 7 with $E_c=0.009$ Ry and $\Delta=0.018$ Ry ($A/a_B=B/a_B^2=1$ Ry) and the approximate positions of the Fermi levels at $T=0$ K (dotted lines) for *Cd*Hg (2 at. % Hg), Cd, and *Cd*Mg (3 at. % Mg).

*Cd*Hg ($x$ at. % Hg) regime, to roughly $x=7$ at. % Hg (see Fig. 1). Hence, we evaluate a shift of the position of the cusp of

$$(110\text{ K})(1.23\text{ at. \%}/7\text{at. \%})=20\text{ K}$$

toward lower temperature in the *Cd*Hg (1.23 at. % Hg) sample.

In Fig. 9 the isotropic $K_\mu(T)$ in the *Cd*Hg sample is shown for temperatures from 4.2 to 337 K. In this sample the cusp is actually located at about 80 K, i.e., 30 K below 110 K, in fair agreement with the crude estimate of the expected temperature shift.

We note that in comparison to Cd the anomalous part of $K_\mu$ is confined to a narrower temperature interval in the *Cd*Hg sample. The fine structure on the right- and left-hand sides, as indicated by dotted lines in Fig. 9, is not clearly statistically evident. However, in view of the observed structure of the anomaly in $K_\mu$ in Cd and *Cd*Mg, the sketched fine structure is a fair interpretation of the data.

As in Cd, $K_\mu$ increases strongly with temperature, and we also observe an appreciable change in the slopes $\partial K_\mu/\partial T$ below and above the cusplike singularity at 80 K.

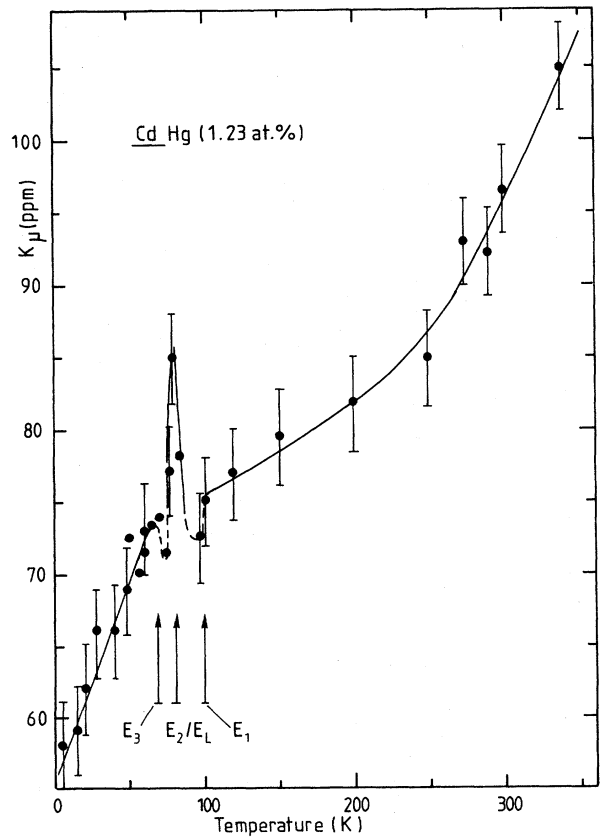


FIG. 9. Isotropic $K_\mu$ in the polycrystalline *Cd*Hg sample between 4.2 and 340 K. The arrows refer to the critical points of the phenomenological three-band model through which the Fermi level is shifted with temperature.

### C. *Cd*Mg

Alloying Cd with isoelectronic Mg, which has a slightly smaller ionic-core radius, reduces the $c/a$ ratio and, consequently, shifts the Fermi level toward higher energies. In Fig. 8 the approximate position of the Fermi level $E_F$

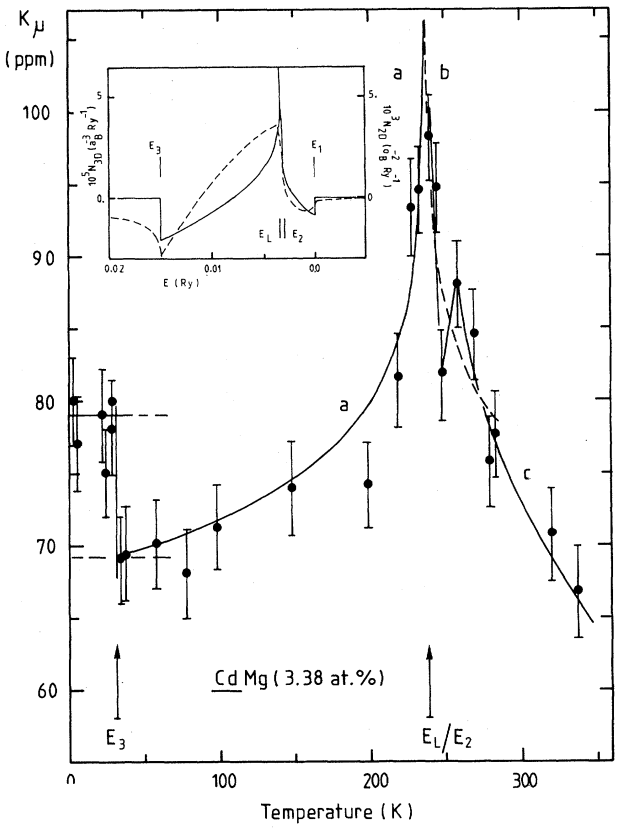


FIG. 10. Isotropic $K_\mu$ in the polycrystalline *Cd*Mg sample between 4.2 and 340 K. The arrow at 32.5 K refers to the finite discontinuity or the $E_3$ critical point, the arrow at 239 K refers to the logarithmic singularity produced by the saddle point at $E_L$ which is nearly degenerate with $E_2$. The solid line ($a$) and the dashed line ($b$) represent the fitted expression $K_\mu(T)=K_0-K_1\ln|T/T_0-1|$, $T_0=239$ K, $K_0=68.5$ ppm, and $K_1=6.22$ ppm. Line $c$ is a guide to the eye. The inset shows the two-dimensional (solid line) and the three-dimensional (dashed line) density-of-states curves associated with the three-band model for the electron states near symmetry point $K$ (from Ref. 7).

in the *Cd*Mg sample relative to the critical points at energies $E_1$, $E_2$, $E_L$, and $E_3$ at symmetry point $K$ is indicated according to Ref. 7. This suggests that the singularity should appear at higher temperatures than in Cd.

The temperature dependence of $K_\mu$ in the polycrystalline *Cd*Mg sample is plotted in Fig. 10. Below 30 K, $K_\mu$ shows a plateau at $+$ (79.0±2) ppm. Somewhere between 30 and 35 K, $K_\mu$ drops sharply by about $-10$ ppm to $+69$ ppm. We assume that this discontinuity in $K_\mu$ occurs at 32.5 K. Above 35 K, $K_\mu$ rises with $T$ by more than $+30$ ppm in the form of a singularity centered at 239 K. The decrease of $K_\mu$ with $T$ above 239 K from 98 to 60 ppm at 339 K follows a similar temperature dependence as the increase below 239 K.

The solid line (*a*) and the dotted line (*b*) in Fig. 10 are fits to a logarithmic singularity of the form

$$K_\mu(T)=K_0-K_1\ln|T/T_0-1|\ ,$$

with (6)

$$K_0=68.4\text{ ppm},\quad K_1=6.2\text{ ppm},\quad T_0=239\text{ K}\ .$$

In order to display this logarithmic behavior more directly, we have plotted the data versus $-\ln|T/T_0-1|$ in Fig. 11. A linear dependence, particularly on the low-temperature side of the singularity, is clearly indicated. This temperature dependence of $K_\mu$ is discussed further in Sec. V. Curve *c* in Fig. 10 connects the data points above 239 K, where, around 260 K, some additional structure very close to the cusp at 239 K might be present.

The interesting aspect of the data obtained in the *Cd*Mg sample is that they reflect essentially the anomalous part of $K_\mu$, which extends over a roughly 8 times wider temperature interval than in pure Cd.

The inset in Fig. 10 displays the fine structure in the density of states $\Delta g(E)$ for electron states in the vicinity of symmetry point $K$ in Cd, as calculated in Ref. 7. As was discussed in Sec. III B, the singularities in $\Delta g(E)$ are associated with the critical points $E_1$ to $E_3$ of the three-band model. The solid line reflects the 2D ($k_x$-$k_y$ plane) and the dashed line the 3D density of states. Clearly, the similarity of $K_\mu$ in the *Cd*Mg sample and the 2D density of states is striking.

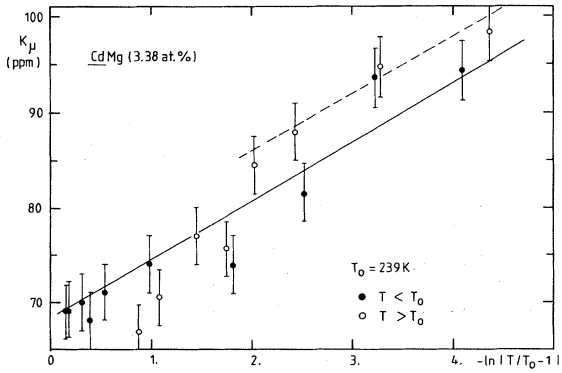


FIG. 11. Plot of $K_\mu$ vs $-\ln|T/T_0-1|$ for the *Cd*Mg sample ($T_0=239$ K). Solid circles refer to the data points in the interval 35 to 239 K below the cusp and open circles refer to the interval 239 to 340 K above the cusp. The solid line corresponds to the fitted curve (*a*) in Fig. 10. The dashed straight line has the same slope as the solid line.

Unfortunately, the temperature dependence of $K_\mu$ above 339 K has not been measured. At higher temperature one expects to find a second discontinuity, similar to the one at 32.5 K but with opposite sign, if the analogy with the density of states holds.

## V. DISCUSSION

### A. Knight-shift contributions

The most general expression for the Knight shift $K_{\rm nuc}$ of a nucleus at a regular lattice site $\vec{r}_0$ is

$$K_{\rm nuc}=\frac{8\pi}{3}\mu_B^2\frac{\Omega_e}{(2\pi)^3}\int_{S_F}|\psi_{\vec{k}}(\vec{r}_0)|^2\frac{dS}{|\,{\rm grad}_{\vec{k}}E(\vec{k})\,|}$$

$$+K_{\rm CP}+K_{\rm dia}\ . \tag{7}$$

The first term is the positive Fermi-contact term, or direct contribution $K_s$, which involves the charge density $|\psi_{\vec{k}}(\vec{r}_0)|^2$ at the site of the hyperfine probe, integrated over all of the electron states on the Fermi surface $S_F$, weighted with their respective density of states $dS/|\,{\rm grad}_{\vec{k}}E(\vec{k})\,|$. $\Omega_e$ is a normalization volume and $\mu_B$ is the Bohr magneton. $K_{\rm CP}$ represents the term called the core-polarization contribution. Its sign can be negative or positive depending on exchange and correlation between the "core" states and the spin-polarized conduction electrons. $K_{\rm dia}$ denotes the diamagnetic screening contribution.

Whenever ${\rm grad}_{\vec{k}}E(\vec{k})=0$, i.e., at critical-energy points on the Fermi surface, one expects a singularity in the density of states and thus in $K_s$. To our knowledge, nuclear Knight-shift measurements have not displayed such effects. The Fermi surface $S_F$ can be split into the small surface element $\delta S$ around a critical point $E_{\rm cr}$ and the complement $S_F-\delta S$. The direct contribution $K_s$ then reads

$$K_s=\frac{8\pi}{3}\mu_B^2\frac{\Omega_e}{(2\pi)^3}\left[\int_{S_F-\delta S}+\int_{\delta S}\right]$$

$$\times|\psi_{\vec{k}}(\vec{r}_0)|^2\frac{dS}{|\,{\rm grad}_{\vec{k}}E(\vec{k})\,|} \tag{8}$$

$$\cong K_{\rm bg}+\frac{8\pi}{3}\mu_B^2\langle|\psi_{\vec{k}}(\vec{r}_0)|^2\rangle_{\delta S}\Delta g(E_F)\ . \tag{9}$$

In Eq. (9) we have assumed that $|\psi_{\vec{k}}(\vec{r}_0)|^2$ is a smooth function over $\delta S$. $K_{\rm bg}$ is a background term involving all electrons on the Fermi surface not associated with critical points, and

$$\Delta g(E_F)=\frac{\Omega_e}{(2\pi)^3}\int_{\delta S}\frac{dS}{|\,{\rm grad}_{\vec{k}}E(\vec{k})\,|} \tag{10}$$

denotes the excess contribution to the density of states

near critical points.

If we now consider an interstitial hyperfine probe which does not disturb the electronic structure of the host at all, Eqs. (7)—(10) are still valid in describing the Knight shift of this hypothetical probe, since the Bloch-function character of the electron states is not destroyed. The neutron could act as such a hypothetical probe, but unfortunately it cannot be fixed at an interstitial site. Turning now to the positive muon as an interstitial probe, one is faced with the situation that the implanted $\mu^+$ introduces a strongly disturbing Coulomb potential which destroys the periodicity of the crystal potential. The electron states near the $\mu^+$ are expected to lose their Bloch-function character and the wave vectors $\{\vec{k}\}$ are no longer good quantum numbers. Consequently, Eq. (7) is not expected to be a generally valid expression for the $\mu^+$ Knight shift. This raises the question of to what extent band-structure features could still be manifest in the $\mu^+$ Knight shift. Deferring a further discussion of this point to the next section, here we merely note that it is still meaningful to work with the concept of a local density of states, defined at the muon site and responsible for a locally defined susceptibility. In this respect, Eq. (9) remains a valid expression also for the $\mu^+$ Knight shift, neglecting for the sake of simplicity any possible core-polarization contribution $K_{CP}$.

### B. Anomalies in $K_\mu$

In the *Cd*Mg sample the finite discontinuity at 32.5 K and the logarithmic singularity at 239 K obviously share all of the features of two-dimensional Van Hove singularities introduced in Sec. II B. The singularities in Cd and in the *Cd*Hg sample showing a cusplike maximum and closely spaced minima to the low- and high-temperature sides of the cusp are likewise attributed to a logarithmic singularity and to two discontinuities, which—in comparison to the results in the *Cd*Mg sample—are compressed into a much smaller temperature range. Assuming that the anomalous features of $K_\mu$ are indeed manifestations of Van Hove singularities, they must obviously be scanned by shifting the Fermi energy with temperature over peculiar points in the local density of states according to

$$K_\mu(T)=K_{bg}(T)+K'\Delta g\left[E_F^0+\frac{\partial E_F}{\partial T}T\right]. \tag{11}$$

Here $E_F^0$ is the Fermi level at $T=0$ K and $\partial E_F/\partial T$ is the phenomenological temperature coefficient of the Fermi level. The background term is now redefined to also include $K_{dia}$ and some presumably small $K_{CP}$.

In Figs. 12(a)—12(c) we plot the anomalous part, $\Delta K_\mu=K_\mu-K_{bg}$, of the muon Knight shift in two different monocrystalline Cd samples and in the polycrystalline *Cd*Hg sample. The background term $K_{bg}(T)$ is assumed to be linear with $T$ over the small temperature range of the anomalous structure. $K_{bg}$ was determined from interpolation between the low-temperature maximum of $K_\mu(T)$ on the left-hand side of the cusp and a few high-temperature data points not too close to the dip in $K_\mu(T)$ on the right-hand side of the cusp. A compilation of the approximate temperatures where the anomalies in $K_\mu$ are located is given in Table III.

The close resemblance of the anomalous $\mu^+$ Knight shift to the density of states associated with the electron states near symmetry point $K$ as shown in Fig. 10 suggests that the singularities in the $\mu^+$ Knight shift may likewise be discussed phenomenologically on the basis of an analogous "three-band model" with "critical points" $E_1,(E_2,E_L),E_3$ close to the Fermi level $E_F$. The physical foundation for such a model, however, thereby remains obscure at this point. Thus, the low-temperature discontinuity is identified with the critical energy point $E_3$, the logarithmic singularity with $E_L$, which effectively coincides with and dominates the singularity associated with $E_2$ and the high-temperature discontinuity with $E_1$. In further discussion we always assume $E_2\approx E_L$. This assignment is consistent with the observed shift of the Fermi level $E_F$ with temperature in the host metals. It was previously mentioned that $E_F$ moves toward lower ener-

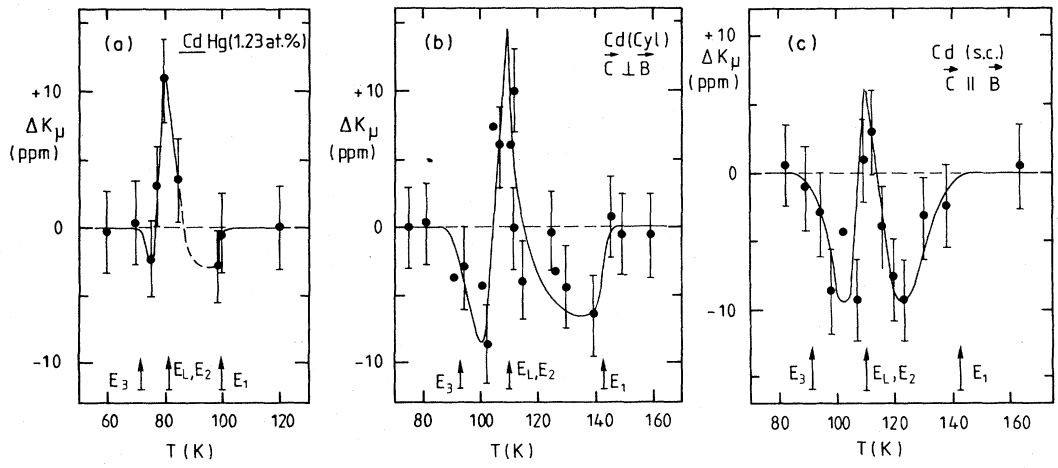


FIG. 12. Anomalous muon Knight shift part $\Delta K_\mu=K_\mu-K_{bg}$ corrected for a background contribution $K_{bg}$ assumed to be linear in temperature. (a) For the *Cd*Hg sample, (b) for the cylindrical Cd sample and the orientation of the applied field perpendicular to the $c$ axis, and (c) for the *Cd*(SC) sample with the applied field parallel to the $c$ axis.

TABLE III. Approximate temperatures associated with the passage of the Fermi level $E_F$ through the critical energy points $E_1$, $(E_2,E_L)$, and $E_3$ from the muon Knight shift in Cd and its alloys.

| Sample | $E_3$ (K) | $(E_2,E_L)$ (K) | $E_1$ (K) |
|---|---|---|---|
| *Cd*Hg (1.23 at.% Hg) | 70 | 80 | 100 |
| pure Cd | 92 | 110 | 140 |
| *Cd*Mg (3.38 at.% Mg) | 32.5 | 239 | |

gies when the axial ratio $c/a$ is increased. Thermal-expansion data[31,32] establish that the $c/a$ ratio increases in Cd and its dilute alloys in the chosen concentration regime. This can also be seen by comparing the temperature dependence of the Cd susceptibility[6] with the concentration dependence of the low-temperature susceptibility in *Cd*Hg alloys,[8] and similarly, in the *Cd*Mg sample where the temperature dependence of the susceptibility[9] parallels the low-temperature susceptibility of *Cd*Mg alloys as a function of the Mg concentration (Fig. 1).

The steeper slope $\partial K_\mu/\partial T$ at the low-temperature side of the cusp, compared to its value above the cusp in the *Cd*Hg sample and in pure Cd, can qualitatively also be understood in terms of the three-band model if one assumes that the upper $E_3$ band is narrower than the lower $E_1$ band. One then expects, for the upper band, a larger change in the density of states for the same energy shift of the Fermi level $E_F$ than in the lower band. The nearly equal drop in $\Delta K_\mu$ on the left- and right-hand sides of the cusp in Figs. 12(b) and 12(c) can be explained in terms of a similar curvature at the "critical points" $E_1$ and $E_3$.

The position of the Fermi level $E_F^0$ at $T=0$ K relative to the critical points on an arbitrary energy scale can be obtained as follows (see Fig. 13): The energy interval $[(E_2,E_L),E_3]$ corresponds to a certain temperature interval $[T_2,T_3]$, as deduced from the position of the anomalies in the various probes [scales (a)—(c) in Fig. 13]. The position of the Fermi energy at 0 K can now be estimated by assuming that the Fermi energy varies linearly with temperature: $E_F(T)=(\partial E_F/\partial T)T+E_F^0$. The temperature coefficient $\partial E_F/\partial T$ is determined from the ratio $|(E_2,E_L)-E_3|/|T_2-T_3|=\partial E_F/\partial T$. Extrapolation

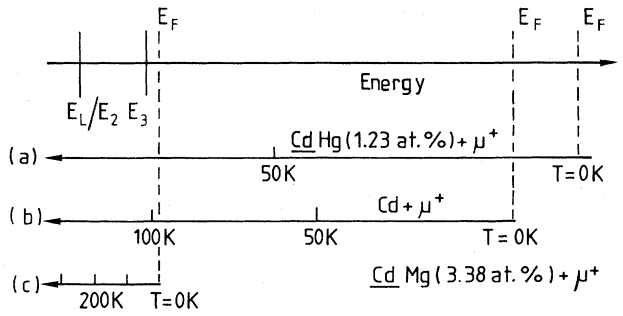


FIG. 13. Position of the critical energy points $(E_2,E_L)$ and $E_3$, and the Fermi levels at $T=0$ K on an arbitrary energy scale as deduced from $K_\mu$ in the *Cd*Hg (1.23 at.% Hg) sample, (b) pure Cd, and (c) the *Cd*Mg (3.38 at.% Mg) sample. Note that the temperature scale is different for each system.

to $T=0$ K fixes the position of $E_F^0$ on the top scale of Fig. 13. The different temperature intervals over which the anomalous $K_\mu$ extends might be a consequence of differences in the apparent "level spacings" or of differences in the thermal-expansion coefficients of pure Cd and the *Cd*Hg and *Cd*Mg alloys, as is evident from

$$\frac{\partial E_F}{\partial T}=\frac{\partial E_F}{\partial(c/a)}\frac{\partial(c/a)}{\partial T}\,.$$

The temperature dependence of the $c/a$ ratio for Cd is found in Ref. 31. For the *Cd*Mg (3.38 at.% Mg) sample, the temperature dependence of the $c/a$ ratio is estimated by interpolating results on the lattice parameters at various temperatures and for various Mg concentrations given in Refs. 31 and 32. From this, one deduces only a somewhat reduced temperature coefficient $\partial(c/a)/\partial T$ of the $c/a$ ratio in *Cd*Mg (3.38 at.% Mg) as compared to pure Cd. This also indicates that the larger temperature interval over which the anomalous $K_\mu$ extends in the *Cd*Mg sample as compared to pure Cd is mainly a consequence of a larger level splitting in the phenomenological three-band model.

For an absolute calibration of the spacings of the critical energies and the position of the Fermi level at $T=0$ K one needs to know $\partial E_F/\partial T$ in absolute energy units per unit temperature. A rough estimate of this temperature coefficient can be obtained if one compares the temperature dependence of the total susceptibility $\chi_{||}(T)$ with the concentration dependence of the low-temperature susceptibility in *Cd*Hg and *Cd*Mg alloys following McClure *et al.*[7] (see Fig. 1). The temperature dependence of $\chi_{||}(T)$ for Cd is found in Ref. 6. For our *Cd*Mg (3.38 at.% Mg) sample we use the published $\chi_{||}(T)$ data for *Cd*Mg (3 at.% Mg) found in Ref. 9.

Correlating the change in slope of $\chi_{||}(T)$ in pure Cd at about 110 K with that in $\chi_{||}(x$ at.% Hg) at $x=7$ at.% Hg (see Fig. 1), we obtain, with the use of the energy scale in Fig. 1, a scaling factor $\partial E_F/\partial T=0.0016$ Ry/110 K$=1.45\times10^{-5}$ Ry/K. Similarly, if we identify the minimum of $\chi_{||}(T)$ in *Cd*Mg (3 at.% Mg) at 200 K, with the minimum of $\chi_{||}(x$ at.% Mg) at $x=0.5$ at.% Mg (see Fig. 1), the scaling factor becomes $\partial E_F/\partial T=0.0039$ Ry/200 K$=1.95\times10^{-5}$ Ry/K. Using, for the *Cd*Hg sample, the same scaling factor as for pure Cd, the critical-energy positions are determined and are collected in Table IV, together with the derived "band parameters" $E_c=(E_2+E_3)/2$ and $\Delta/3=(E_3-E_2)/2$ relevant for the three-band model, where $E_2\approx E_L$. The same scaling factors and Table IV were used in drawing Fig. 14, which shows the calculated position of the critical energies relative to the Fermi levels at $T=0$ K as deduced from $\Delta K_\mu(T)$. The Fermi level itself, of course, is not affected by the presence of a single muon. As shown in Refs. 33 and 34 the induced shift of the Fermi level as a function of hydrogen concentration is zero in the dilute limit, i.e., $\partial E_F/\partial x=0$ for $x\to0$.

In the preceding discussion it was shown that the anomalous muon Knight shift in Cd, *Cd*Hg, and *Cd*Mg finds a consistent explanation in terms of a three-band model similar to the one which describes the electron states near the symmetry point $K$ of the host metals with

TABLE IV. Critical energies $E_1, E_{2,L}, E_3$ and band parameters $E_c$ and $\Delta$ following from the critical temperatures given in Table III. The origin of the energy scale is $E_1$ (or $E_F^0$: values in parentheses).

| Sample | $E_1$ (mRy) | $E_2, E_L$ (mRy) | $E_3$ (mRy) | $E_c$ (mRy) | $\Delta/3$ (mRy) |
|---|---|---|---|---|---|
| *Cd*Hg (1.23 at.% Hg)[a] (inside $\mu^+$ cell) | 0.0 (−1.45) | 0.29 (−1.16) | 0.44 (−1.02) | 0.36 | 0.075 |
| Cd (inside $\mu^+$ cell)[a] | 0.0 (−2.03) | 0.44 (−1.60) | 0.70 (−1.33) | 0.57 | 0.13 |
| *Cd*Mg (3.38 at.% Mg)[b] ($T > 360$ K) (inside $\mu^+$ cell) | 0.0 ($< -7.0$) | $> 2.3$ (−4.66) | $> 6.3$ (−0.63) | $> 4.3$ | 2.0 |
| bulk Cd (see Fig. 1)[c] | 0.0 (−0.75) | 3.00 (+2.25) | 15.0 (+14.25) | 9.0 | 6.0 |

[a]Parameters evaluated with $\partial E_F/\partial T = 1.45 \times 10^{-5}$ Ry/K.
[b]Parameters evaluated with $\partial E_F/\partial T = 1.95 \times 10^{-5}$ Ry/K.
[c]From Ref. 7.

critical points $E_1, (E_2, E_L), E_3$. The apparently predominant two-dimensional character of the observed Van Hove singularities must be a consequence of a very weak dependence of the "band energy" on the wave-vector component $k_z$.

Now, one has to justify the adopted "band model" in explaining a local property at the site of a strongly perturbing probe and, perhaps, to relate the "three-band model" to known properties of the Cd band structure. The problem that arises stems from the use of conflicting concepts invoking band states in the discussion of local properties at an impurity site. We are not able to solve this conflict and we could not find any reference to a similar problem in the literature. In this respect, the $\mu^+$ data are unique and may call for a novel theoretical approach. Nevertheless, in the following discussion we try to forward plausible conclusions relying strongly on analogies.

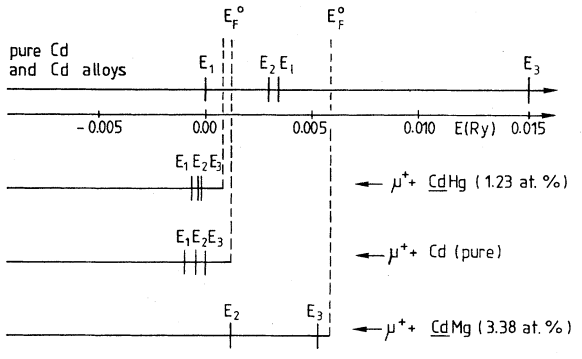


FIG. 14. Critical energies $E_1$, $(E_2, E_L)$, and $E_3$ of Cd and Cd alloys and the position of the Fermi level $E_F^0$ at 0 K for *Cd*Hg (1.23 at.% Hg), Cd, and *Cd*Mg (3.38 at.% Mg) in Ry according to Ref. 7, in comparison with the critical points relevant for the muon Knight shift calculated with the scaling factors $\partial E_F/\partial T$ given in the text and the critical temperatures give in Table III.

It is striking that the anomalous $\mu^+$ Knight shift can be explained on the basis of a three-band model which seems to reflect qualitatively all features of the Cd band structure in the vicinity of symmetry point $K$, as discussed in Sec. III. This concerns the number of singularities, the types of singularities, the relative order of the levels, and the weak $k_z$ dependence of the band energy close to symmetry point $K$. It thus seems that $K_\mu$ originates to quite an extent from electron states near symmetry point $K$, which implies a high density of these electrons at the $\mu^+$ interstitial site. This is consistent with the fact that the nuclear Knight shift in Cd (Ref. 10) and in Cd alloys (Ref. 35), sampling at the regular lattice site, does not display any anomalies or singularities as a function of temperature. Theoretical calculations by Kasowski[11] show that the Cd nuclear Knight shift originates exclusively from Fermi-surface electrons in regions of the Brillouin zone around the symmetry point $\Gamma$ and the symmetry point $M$, but not from the symmetry point $K$.

However, comparing the apparent spacings of the critical energies and their relative position to the Fermi level at $T=0$ K, as deduced from the anomalous $\mu^+$ Knight shift, with the Cd band structure at symmetry point $K$, one notices significant differences (see Fig. 14). With regard to the band structure, the Fermi energy at $T=0$ K in Cd, *Cd*Hg, and *Cd*Mg is well below the upper critical point $E_3$. By increasing the temperature it will not be possible to shift $E_F$ through this critical point. A temperature increase will always shift the Fermi level to lower energies. In Cd and *Cd*Hg it will be possible to shift $E_F$ through the critical point $E_1$ and, in *Cd*Mg, through $(E_2, E_L)$ and $E_1$. The accompanying change in the Fermi-surface topology was termed an electron, or Lifshitz, phase transition. In contrast, the fact that one observes all three critical points in the $K_\mu$ data implies that they are all below the Fermi energy at $T=0$ K. Moreover, the splitting of the critical points in the $K_\mu$ data varies considerably between the *Cd*Hg, Cd, and

*Cd*Mg samples. The width of the anomalous structure increases from *Cd*Hg to Cd to *Cd*Mg. The center of the structure, roughly defined by the logarithmic singularity, shifts to higher temperatures upon going from *Cd*Hg to Cd and from Cd to *Cd*Mg. With respect to the position of the Fermi level at $T=0$ K, the entire anomalous structure is shifted toward lower energies. Qualitatively, the same tendency is inferred from the rigid three-band model for the band structure of Cd and its alloys in the vicinity of symmetry point $K$. Although the observed splittings and the positions of the critical points relative to $E_F^0$ in the $K_\mu$ data are different from the ones in the band structure of Cd and its alloys, the similarities are persuasive enough to propose that the anomalous muon Knight shift originates precisely from these states. If so, one has to conclude that inside the muon cell these states appear reduced in splitting, lowered in energy, and pulled down below $E_F^0$ as compared to the bulk situation. This would constitute a new and unanticipated effect. Figure 14 shows that the apparent energy shifts in the present case are of the order of $-10$ mRy. It seems impossible, however, to obtain such shifts inside the muon cell with the short-ranged screened muon impurity potential, which is expected to act just like an elastic scattering center on the Bloch waves, shifting their phases, but leaving their energy unchanged.

In contrast to the case of a single $\mu^+$ or proton impurity in a metal, where no lowering of energy levels is expected (not even locally), metal-hydrogen systems exhibit a lowering of host electron states with $s$ character relative to the proton site, which is a consequence of the hydrogen-induced lowering of the overall potential.[36–43] The latter is not to be confused with the observed shifts in the present study.

The absence of any narrow structures in the temperature dependence of $K_\mu$ in Zn is consistent with the above discussion of the results in Cd and its alloys. In contrast to Cd, in pure Zn the Fermi energy at 0 K is above the critical point $E_3$. If in the presence of a $\mu^+$, $E_3$ inside the $\mu^+$ cell is shifted down by about the same amount as in Cd and its alloys ($\sim 10$ mRy), it may not be possible to shift $E_F$ across the critical points ($E_3$,$E_{2,L}$,$E_1$) even by increasing the temperature up to the melting point.

The question arises, of course, whether other mechanisms could be responsible for the kind of sharp anomalies displayed by the temperature dependence of the $\mu^+$ Knight shift in Cd and the alloys *Cd*Hg and *Cd*Mg, whereby the reader is reminded that the nuclear Knight shift in Cd already has an unusual, strong temperature dependence. Since it is known that the self-trapping and diffusion properties of $\mu^+$ in metals are extremely sensitive to structural features and imperfections of the host, one might wonder, in particular, whether they are also the origin of the observed Knight-shift anomalies. However, from the fact that the anomalies are observed at relatively high temperatures, where diffusion, trapping, and detrapping rates are known to follow an almost classical, temperature-activated Arrhenius behavior,[44] it appears impossible to explain the extremely narrow structure of the anomalies in Cd and *Cd*Hg (1.23 at.% Hg) on such grounds. In particular, it appears impossible to reproduce the "cusplike" singularity observed in all of the data. As has been demonstrated in Zn,[28] $\mu^+$ trapping at lattice defects can indeed lead to a pronounced temperature dependence of the $\mu^+$ Knight shift, but never to the narrow structures observed in Cd and its alloys.

On the other hand, one might ask whether the anomalies could be related to properties of the Cd host other than the electronic properties already discussed. To our knowledge no drastic changes in the bulk properties of Cd and the alloys *Cd*Hg and *Cd*Mg are reported in the literature near any of the critical temperatures listed in Table III.

### C. Anisotropic muon Knight shift

Trivial contributions due to the demagnetization field $\vec{B}_{dm}$ and the Lorentz field $\vec{B}_L$ to $K_{ax}$ are eliminated since, for the present investigations, we have used spherical samples, for which $\vec{B}_{dm}$ and $\vec{B}_L$ cancel each other. Hence, the anisotropy observed must be an intrinsic property of $K_\mu$.

The anisotropic or axial part $K_{ax}$ of the Knight shift may generally be written as a sum of three contributions,

$$K_{ax}=K_{ax}^{(dip)}+K_{ax}^{(SS)}+K_{ax}^{(dia)} .$$

Here, $K_{ax}^{(dip)}$ is the dipolar hyperfine contribution characterizing the quadrupole moment of the electron distribution around the muon. It originates from the dipole-dipole interaction between the muon spin and the spin of the conduction electrons at the Fermi surface, and vanishes only when the relevant ensemble symmetry of the muons is cubic. $K_{ax}^{(SS)}$ arises from the anisotropic spin susceptibility or the anisotropic $g$ factor, respectively, of the conduction electrons, in connection with the isotropic Fermi-contact interaction. $K_{ax}^{(dia)}$ denotes an eventual anisotropic contribution from the diamagnetic screening[45] and is expected to be small and temperature independent.

We first consider the dipolar contribution $K_{ax}^{(dip)}$ and assume that it is dominant in the observed $K_{ax}$. The temperature dependence of $K_{ax}$ in Fig. 7 may then indicate a change in the symmetry character of the electron distribution around the muon. At 110 K, where $K_{ax}$ vanishes, the electron distribution would possess spherical symmetry. Below 110 K, where $K_{ax}$ is negative, the electron distribution would have an oblate shape concentrated in the basal plane of the Cd lattice. The positive sign above 110 K would indicate a prolate electron distribution concentrated along the $c$ axis. A similar change in sign of $K_{ax}$, between 40 and 70 K, has been observed in the Cd nuclear Knight shift[10] [Fig. 3(b)]. $K_{ax}$ of the nuclear Knight shift is small and negative at 4.2 K and increases continuously with temperature up to the melting point. Kasowski[11] proposed an explanation for the temperature behavior of the axial nuclear Knight shift based on the effect of the electron-phonon interaction on the Cd pseudopotentials. He postulates that the strongly-temperature-dependent $p_x$-$p_y$ orbital of the $M$-centered electron states is increasingly destroyed with rising temperature. At low temperature, the contribution of the $M$-centered electron states is nearly cancelled by the $p_z$ orbital of the $\Gamma$-centered electron states, which is nearly temperature independent. However, in the case of the muon Knight shift, the van-

ishing of $K_{ax}$ at 110 K correlates with the cusp singularity or the passage of the Fermi level through the critical points $E_L, E_2$ in the three-band model. Therefore, the negative sign below 110 K probably reflects a property of the electron states of the upper, or $E_3$, band, and the positive sign above 110 K a property of the states of the lower, or $E_1$, band. The dipolar coupling is generally weaker[46] than the Fermi-contact interaction and a small $K_{ax}/K_{iso}$ ratio (after correcting $K_{iso}$ for the diamagnetic screening contribution ) can imply a large non-$s$ character of the electrons at the Fermi level with respect to the interstitial $\mu^+$. In Cd at $T=20$ K we find $K_{ax}/K_{iso}\simeq -4.5\%$, and at $T=500$ K, $K_{ax}/K_{iso}\simeq +1.6\%$ (with a $-20$-ppm diamagnetic screening correction in $K_{iso}$). These values are of the same order as those for the nuclear Knight shift with $K_{ax}/K_{iso}\simeq -3\%$ at $T=4.2$ K and $K_{ax}/K_{iso}= + 10\%$ at $T=500$ K. On the other hand, theoretical calculations of the charge distribution around hydrogen in metals[3] show that the strong proton potential is essentially screened by electron states with a dominant $s$ character relative to the proton. Experimentally, Wampler *et al.*[4] found, from measurements of the Dingle temperature in the de Haas–van Alphen effect in dilute *Cu*H alloys, that the screened proton is predominantly a short-range, structureless isotropic scattering center for the conduction electrons.

However, if the measured Knight shift is only of the Fermi-contact type, which itself is isotropic by nature, the temperature-dependent axial part, $K_{ax}$, of $K_\mu$ must orignate from an anisotropic spin susceptibility. An anisotropic spin susceptibility can be related to an anisotropic $g$ factor of the relevant conduction electrons. In this case, we may write[47]

$$(K_{||}-K_\perp)/K_{iso}\cong \tfrac{1}{3}(g_{||}-g_\perp)/g_{iso} ,$$

where $g_{||}$ and $g_\perp$ refer to the $g$ factor with the field parallel and perpendicular to the $c$ axis, respectively. At 110 K, where $K_{ax}$ vanishes, $g_{||}$ and $g_\perp$ would be of equal magnitude, whereas below and above 110 K, $g_{||}$ and $g_\perp$ would be different. Since the disappearance of $K_{ax}$ correlates with the cusplike singularity or the passage of the Fermi level through the critical points $E_L, E_2$, we must conclude that the relative magnitude of $g_{||}$ and $g_\perp$ is a consequence of the position of $E_F$ relative to the critical points or the bands in our phenomenological three-band model. The situation at low temperature, where the Fermi level lies above the critical point $E_3$ in the phenomenological three-band model, corresponds exactly to the situation realized at $T=0$ K in the band structure of hcp Zn.[5,48] The $g$ factor for the electron pocket states in the upper, or $E_3$, band has been calculated for Zn in Refs. 22 and 47. Experimentally, one finds $g_{||}\simeq 89$ and $g_\perp \ll g_{||}$, which is a consequence of the small effective mass of the $E_3$-band states (see Ref. 22). Obviously, this is not in accord with the negative sign in $K_{ax}$ of the muon Knight shift in Cd below 110 K.

The Pauli spin susceptibility and its anisotropic part in Cd have been calculated by Kar *et al.*[13] using a temperature-dependent pseudopotential. The results for $T=0$, 293, and 469 K lead to a $\chi^P_{||}-\chi^P_\perp$ which is positive at low temperature and negative at high temperature, in contrast to the behavior of the axial part of the muon Knight shift. However, the total Pauli spin susceptibility includes an average over the full Fermi surface and may be expected to differ from the effective susceptibility related to particular electron states at the Fermi surface.

In any case, explaining the strongly-temperature-dependent axial part of the muon Knight shift constitutes an interesting and challenging theoretical problem.

### D. Comparison of the low-temperature $K_\mu$ with jellium calculations

The Knight-shift value extrapolated to $T=0$ K in the polycrystalline Cd sample amounts to $(48\pm 4)$ ppm. This value is in fair agreement with values calculated by Manninen[2] within the framework of the spherical solid model. By using a fcc lattice with the same nearest-neighbor distance to the muon as in the hcp lattice of Cd, he found values of 54 ppm for the tetrahedral site and 74 ppm for the octahedral site. The pure-jellium model, including the diamagnetic screening, in contrast, gives a much larger value of 103 ppm.[2]

## VI. SUMMARY

In this work it has been shown that the Knight shift of a light hydrogen isotope at an interstitial site may strongly be influenced by details in the band structure of the host metal. In pure Cd and in *Cd*Hg and *Cd*Mg alloys, this influence results in a pronounced temperature dependence of $K_\mu$ and in the appearance of Van Hove singularities as well as in a strongly temperature-dependent axial contribution. To our knowledge, the present Knight-shift measurements are the first ones in which Van Hove singularities in the local-electron density of states have been directly mapped. The relevant electron density of states is shown to have predominantly 2D character. This follows from a sharp and finite discontinuity in $K_\mu$, typical for 2D minima or maxima, and a logarithmic singularity, typical for a 2D saddle point. The relative sequence and the topological character of the critical points as revealed in the anomalies of $K_\mu$ can be understood in terms of a three-band model which is essentially a replica of the band structure of Cd and its isostructural, isovalent alloys near the symmetry point $K$ of the hexagonal Brillouin zone close to the Fermi energy. A *new and unexpected effect* is thereby revealed, in that the "*locally*" probed band structure, as compared to the bulk band structure of the pure metal, shows a downshift in energy relative to the Fermi energy and an apparent renormalization of the energy scale. The shift and the change in energy scale are different for the three systems investigated. A conceptually consistent explanation for these results has not yet been found. In terms of the screened muon impurity potential, which is *short ranged* and expected to behave as an *energy-conserving* scattering center, the apparent lowering and reduced separation of electron states may be difficult to understand. The influence of the alloy composition on the splitting of the states, i.e., on the parameters $E_c$ and $\Delta$, is also completely mysterious. It is conjectured that a long-range potential, perhaps related to the induced lattice strain around the $\mu^+$, in conjunction with associated diffraction processes of conduction electrons, may provide a mechanism for the explanation of the present results.[49] A

theoretical analysis in this direction is being initiated, but other possible mechanisms need to be explored as well.

## ACKNOWLEDGEMENTS

We gratefully acknowledge helpful and stimulating discussions with T. M. Rice and H. R. Ott, Eidgenössische Technische Hochschule Zürich, (ETHZ). During the measurements we enjoyed the help of W. Rüegg (ETHZ) and H. Wehr (Universität Mainz). This work was supported in part by the Schweizerisches Institut für Nuklearforschung (SIN). The present paper is based on the doctoral thesis of one of the authors (W. Studer).

[1]A. Schenck, Helv. Phys. Acta **54**, 471 (1981).
[2]M. Manninen, Phys. Rev. B **27**, 53 (1983).
[3]M. Gupta and A. J. Freeman, Phys. Rev. B **17**, 3029 (1978).
[4]W. R. Wampler and B. Lengler, Phys. Rev. B **15**, 4614 (1977).
[5]R. W. Stark and L. M. Falicov, Phys. Rev. Lett. **19**, 795 (1967).
[6]J. A. Markus, Phys. Rev. **76**, 621 (1949).
[7]J. W. McClure and J. Martyniuk, Phys. Rev. Lett. **29**, 1072 (1972).
[8]I. V. Svechkarev and L. B. Kuzmicheva, Phys. Status Solidi **37**, K113 (1970).
[9]B. I. Verkin, L. B. Kuzmicheva, and I. V. Svechkarev, Zh. Eksp. Teor. Fiz. **54**, 74 (1968) [Sov. Phys.—JETP **27**, 41 (1968)].
[10]For references, see G. C. Carter, L. H. Bennet, and D. J. Kahan, *Metallic Shifts in NMR*, (Pergamon, Oxford, 1977), Pt. 1.
[11]R. V. Kasowski, Phys. Rev. **187**, 891 (1969).
[12]N. C. Das, Phys. Rev. B **20**, 1288 (1979).
[13]K. Kar and N. C. Das, Phys. Rev. B **19**, 441 (1979).
[14]J. H. Ziman, Adv. Phys. **16**, 421 (1967).
[15]N. A. Galaktionowa, *Hydrogen Metal Systems Data Book* (Ordentlich, Holon, Israel, 1980).
[16]E. Klempt, R. Schulze, H. Wolf, M. Camani, F. N. Gygax, W. Rüegg, A. Schenck, and H. Schilling, Phys. Rev. D **25**, 652 (1982).
[17]A. J. Bennet and L. M. Falicov, Phys. Rev. **136**, A998 (1964).
[18]There is an inconsistency between the values $E_c$ and $\Delta$ ($E_c=0.009$ Ry and $\Delta=0.012$ Ry) quoted in the text and the values following from the Fig. 1 of Ref. 7. We have used the latter ($E_c=0.009$ Ry and $\Delta=0.018$ Ry).
[19]L. Van Hove, Phys. Rev. **89**, 1189 (1953).
[20]J. C. Phillips, Phys. Rev. **104**, 1263 (1956).
[21]I. M. Lifshitz, Zh. Eksp. Teor. Fiz. **38**, 1569 (1960) [Sov. Phys.—JETP **11**, 1130 (1960)].
[22]D. C. Tsui and R. W. Stark, Phys. Rev. Lett. **16**, 19 (1966).
[23]E. Zaremba and D. Zobin, Phys. Rev. B **22**, 5490 (1980).
[24]F. N. Gygax, W. Rüegg, A. Schenck, H. Schilling, W. Studer, and R. Schulze, J. Magn. Magn. Mater. **15-18**, 1191 (1980).
[25]F. N. Gygax, A. Hintermann, W. Rüegg, A. Schenck, and W. Studer, Solid State Commun. **38**, 1245 (1981).
[26]F. N. Gygax, A. Hintermann, W. Rüegg, A. Schenck, W. Studer, A. J. van der Wal, and L. Schlapbach, in Proceedings of the Yamada Conference on Muon Spin Rotation (Shimoda, Japan, 1983) Hyperfine Interact. **17—19**, 377 (1984).
[27]H. Wehr, K. Knorr, F. N. Gygax, A. Hintermann, A. Schenck, and W. Studer, J. Phys. F **13**, 885 (1983).
[28]F. N. Gygax, A. Hintermann, W. Rüegg, A. Schenck, W. Studer, A. J. van der Wal, and H. Wehr, Phys. Rev. Lett. **51**, 505 (1983).
[29]The angular dependence published in Ref. 30 showed strongly irreproducible features at low temperatures which we attribute to the particular sample used in the early measurements. In the present measurements care was taken to adjust the temperature sufficiently slowly to avoid strains in the Cd sample with its strongly anisotropic thermal-expansion coefficients. This procedure always led to reproducible data.
[30]F. N. Gygax, A. Hinterman, W. Rüegg, A. Schenck, and W. Studer, Hyperfine Interact. **8**, 479 (1981).
[31]D. E. Edwards, W. E. Wallace, and R. S. Craig, J. Am. Chem. Soc. **74**, 5256 (1952).
[32]W. Hume-Rothery and G. V. Raynor, Proc. R. Soc. London, Ser. A **74**, 471 (1939).
[33]J. Friedel, Adv. Phys. **3**, 446 (1945).
[34]E. A. Stern, Phys. Rev. B **5**, 366 (1972).
[35]V. V. Zhukov, I. D. Weisman, and L. H. Bennet, J. Res. NBS, Sect. A **77**, 713 (1973).
[36]A. C. Switendick, Ber. Bunsenges. Phys. Chem. **76**, 535 (1972).
[37]D. E. Eastman, J. K. Cashion, and A. C. Switendick, Phys. Rev. Lett. **27**, 35 (1971).
[38]F. Antonangeli, A. Balzarotti, A. Bianconi, E. Burrattini, P. Perfetti, and N. Nistico, Phys. Lett. **55A**, 309 (1975).
[39]L. Schlapbach and J. P. Burger, J. Phys. (Paris) Lett. **43**, L273 (1982).
[40]D. E. Eastman, Solid State Commun. **10**, 933 (1972).
[41]Y. Fukai, S. Kazama, K. Tanaka, and M. Matsumoto, Solid State Commun. **19**, 507 (1976).
[42]E. Gilbert, Phys. Status Solidi B **69**, 477 (1975).
[43]R. Griessen and L. M. Huisman, in *Electronic Structure and Properties of Hydrogen in Metals,* edited by P. Jena and E. B. Satterthwaite (Plenum, New York, 1983).
[44]D. Richter, in *Neutron Scattering and Muon Spin Rotation,* Vol. 101 of *Springer Tracts in Modern Physics,* edited by G. Höhler (Springer, Berlin, 1983).
[45]J. Keller and W. Baltensberger, Int. J. Quantum Chem. **14**, 123 (1980).
[46]N. Bloembergen and T. J. Roland, Acta Metall. **1**, 731 (1953).
[47]A. Rubens, B. de Castro, and R. T. Schuhmacher, Phys. Rev. B **7**, 105 (1973).
[48]J. P. Van Dyke, J. W. McClure, and J. F. Doar, Phys. Rev. B **1**, 2511 (1970).
[49]This idea was suggested to us by Professor T. M. Rice of the Institut für Theoretische Physik der ETH, Zürich, Switzerland.